Quasi-Objective Eddy Visualization from Sparse Drifter Data

Alex P. Encinas Bartos, Nikolas O. Aksamit and George Haller*
Institute for Mechanical Systems
ETH Zürich

May 3, 2022

Abstract

We employ a recently developed single-trajectory Lagrangian diagnostic tool, the trajectory rotation average ($\overline{\text{TRA}}$), to visualize oceanic vortices (or eddies) from sparse drifter data. We apply the $\overline{\text{TRA}}$ to two drifter data sets that cover various oceanographic scales: the Grand LAgrangian Deployment (GLAD) and the Global Drifter Program (GDP). Based on the $\overline{\text{TRA}}$, we develop a general algorithm that extracts approximate eddy boundaries. We find that the $\overline{\text{TRA}}$ outperforms other available single-trajectory-based eddy detection methodologies on sparse drifter data and identifies eddies on scales that are unresolved by satellite altimetry.

Keypoints

- The recently derived trajectory rotation average metric shows potential for highlighting vortical flow structures in sparse velocity data.
- We develop here an algorithm that extracts approximate eddy boundaries from sparse drifter data using the trajectory rotation average.
- We find that the derived rotation metric outperforms other available eddy detection methodologies on sparse drifter data and describes eddy dynamics on scales that are unresolved by satellite altimetry.

Summary

Meso and submesoscales vortices (or eddies) can trap and transport material over large distances, thereby playing a crucial role in the dynamics of our ecosystem. In order to expand our understanding of the transport of marine tracers, we need to accurately and reliably track the evolution of vortical flow structures. Drifter trajectories represent a valuable but sparse source of information for this purpose. We utilize this information here to compute a single-trajectory Lagrangian diagnostic tool, that approximates the local material rotation in the flow. Our findings on two distinct data sets suggest that the selected rotational flow diagnostic accurately highlights material vortices from sparse drifter data.

1 Introduction

Oceanic vortices (or eddies) are highly energetic coherent flow structures which can transport material over large distances. Studying the dynamics of eddies is key to understanding the dispersion of marine tracers, such as biological nutrients and pollutants [63, 15, 4, 42, 2]. Lagrangian eddies, generally referred to as elliptic Lagrangian coherent structures (LCS) in dynamical systems theory [22], are material objects that trap and transport floating particles over large distances in the ocean. The size of such eddies ranges from a few kilometers (submesoscale) to hundreds of kilometers (mesoscale). Mesoscale eddies have predominantly been inferred from the sea-surface-height (SSH) field derived from satellite altimetry data [10, 13, 1]. There is, however, increasing evidence that submesoscale

*Email:georgehaller@ethz.ch

currents on the order of a few kilometers influence the marine ecosystem at least as strongly as mesoscale eddies, especially along coastlines and oceanic fronts [41, 28]. Despite this, submesoscale eddies are rarely studied in detail as their trace in the SSH field is weak. Compared to the SSH field, which only captures the geostrophic velocity component of the ocean, drifters closely follow ocean currents thereby accurately resolving small scale features [35]. As opposed to satellite-based altimetry data, surface drifter observations provide direct and reliable information about the local ocean surface velocity field at very high temporal resolutions. Ocean drifters are, however, sparsely distributed in space, rendering most Lagrangian coherent structure (LCS) diagnostics inapplicable to their trajectories. Indeed, most mathematically justifiable algorithms for the detection of vortical Lagrangian coherent structures (elliptic LCSs) require differentiation with respect to initial conditions [22], which is unfeasible for sparse drifter data.

Alternatively, elliptic LCSs can be viewed as a coherently evolving set of material trajectories in space. Hence, a wide range of clustering methods for extracting elliptic LCSs have been proposed (see [20] for a review). These objective methods fundamentally distinguish themselves depending on the specific clustering algorithm and on the employed distance metric. Common algorithms include fuzzy clustering [16], spectral graph methods [21, 58] and density based clustering methods [43]. Their results, however, rely on user defined input parameters such as the number of clusters, which a priori determines the possible elliptic LCS to be detected by the method in the domain. This limitation becomes even more pronounced for sparse drifters for which the number of eddies is a priori unknown.

Consequently, to extract elliptic LCS from drifter data, one is forced to rely on features of a single trajectory, such as trajectory length, velocity, acceleration and curvature. These features, however, are all inherently non-objective (frame-dependent) quantities whereas LCS, as material objects, are objective, i.e., indifferent to coordinate frame changes [22]. Common single-trajectory methods, such as the absolute dispersion [49], trajectory length [39, 37], Lagrangian spin [57], maximal trajectory extent [44], trajectory complexity [56] and wavelet ridge analysis [29], are limited in capturing elliptic LCSs as they are either non-objective or lack direct physical connection to material deformation in the fluid. Accordingly, while most of these methods were originally introduced to visualize LCSs from truly sparse trajectories, their application to drifter data has remained rare. Notable exceptions include the fully automated looper detection algorithms based on the Lagrangian spin [64, 18, 12, 35]; and the wavelet ridge regression [31]. Both methods seek to extract oscillatory motions from a time-series and lead to comparable results. The methodology employed by [64, 18, 12, 35] is an aggregate measure of rotation within a time-series of the Lagrangian spin, whereas [31] quantifies the instantaneous oscillatory motion of the velocity using signal processing techniques. Loosely speaking, elliptic LCSs are hereby visualized exclusively through looping (or oscillatory) trajectory segments.

In order to distinguish looping from non-looping trajectory segments, a user-defined threshold is inevitably required. In a practical setting, however, differentiating between looping and non-looping trajectories proves to be challenging and hence finding an appropriate parameter is far from trivial. A common approach is to manually tune a threshold value based on a subset of trajectories. Although this provides a natural and intuitive way to characterize elliptic LCSs, a considerable amount of information is lost when discarding non-looping trajectory segments. It would be more desirable to retain all trajectory information and associate to each trajectory a Lagrangian diagnostic related to material rotation in the flow. The rotational diagnostic can then be plotted over the evolving trajectory positions. This approach would provide a qualitative overview of individual vortical flow structures, without relying on any chosen threshold.

Here we propose to identify eddies from sparse drifter data using recent theoretical work by [25] on adiabatically quasi-objective single-trajectory diagnostics. Such diagnostics closely approximate some objective LCS diagnostics in frames satisfying conditions that typically hold in geophysical flows. We show that the adiabatically quasi-objective trajectory rotation average ($\overline{\mathrm{TRA}}$) reveals elliptic LCSs (material eddies) at meso-and submesoscales from sparse drifter trajectory data. We additionally compare the vortical flow features extracted from the drifter-based $\overline{\mathrm{TRA}}$ computation with those obtained from other available Lagrangian single trajectory diagnostics such as the trajectory length [39, 37] and Lagrangian Spin[57, 35]. We further validate the extracted features with respect to Lagrangian averaged vorticity deviation (LAVD) computed from geostrophic ocean velocity fields derived from satellite altimetry data (AVISO). The LAVD is an objective Lagrangian rotation diagnostic which highlights elliptic LCS in densely gridded velocity data.

2 Data

2.1 Satellite altimetry ocean-surface current product (AVISO)

The two-dimensional, satellite-altimetry-derived ocean-surface current product (AVISO) has been the focus of several coherent structure studies [47, 46, 4]. Using this product, the geostrophic velocity $\mathbf{v}_g(\mathbf{x}, t)$ of ocean currents is obtained from the remotely sensed sea-surface height η as

$$\mathbf{v}_g(\mathbf{x}, t) = \frac{g}{f} \begin{pmatrix} 0 & -1 \\ 1 & 0 \end{pmatrix} \nabla \eta(\mathbf{x}, t), \tag{1}$$

where g is the constant of gravity and f is the Coriolis parameter. A global daily-gridded version of the sea-surface height profile with a spatial resolution of $(0.25^\circ \times 0.25^\circ)$ is freely available from the Copernicus Marine Environment Monitoring Service.

2.2 Drifter data sets

While satellite-based altimetry yields mesoscale velocity fields, surface drifter observations provide direct estimates for the local surface velocity field. In order to illustrate the range of applications of the adiabatically quasi-objective single-trajectory rotation measure introduced in [25], we will focus on two drifter data sets: the Grand LAgrangian Deployment (GLAD) and the Global Drifter Program (GDP).

2.2.1 Grand LAgrangian Deployment (GLAD)

We consider the Coastal Dynamics Experiment (CODE) drifters [11], released during the Grand LAgrangian Deployment (GLAD) [46, 48, 40]. In order to study relative dispersion statistics, around 300 drifters were deployed on the $20^{th} - 31^{th}$ of July 2012 in the northern Gulf of Mexico, sampling various submesoscale features over several weeks. The positions of the drifters were reported every 15 minutes from which we estimate their velocities via finite differencing. In order to highlight important circulation features, we focus on GLAD-drifters active from the 10^{th} to the 17^{th} of August, restricting the domain of interest to

$$\{(x, y) \in [89^\circ\mathrm{W}, 86^\circ\mathrm{W}] \times [26^\circ\mathrm{N}, 29^\circ\mathrm{N}], \quad t \in [222 \text{ doy}, 229 \text{ doy}]\}, \tag{2}$$

where doy is in short for days of year.

2.2.2 Global Drifter Program (GDP)

Additionally, we consider the Global Drifter Program (GDP) data set, which contains more than 20,000 drifters released over the past 40 years. At least 1,000 of those drifters are now simultaneously active worldwide [33]. These drifters report their positions every 6 hours. We specifically focus on a subset of drifters active from the 4^{th} September 2006 to the 4^{th} October 2006 in the Gulf Stream, i.e., in the domain

$$\{(x, y) \in [72.5^\circ\mathrm{W}, 65^\circ\mathrm{W}] \times [32.5^\circ\mathrm{N}, 40^\circ\mathrm{N}], \quad t \in [246 \text{ doy}, 276 \text{ doy}]\}. \tag{3}$$

2.2.3 Drifter data preprocessing

As higlighted by [17, 5] and [53], inertial oscillations have little effect on the overall motion of nearby particles as they periodically return to their starting position after one inertial period. The anticyclonic looping arising from inertial oscillations, however impacts the drifter velocity profile without affecting separation between nearby particles. In order to remove this unwanted effect from our analysis, we apply a 6^{th}-order low-pass Butterworth filter to the drifter trajectories with a cut-off period of $T_{cut} = 1.5 T_{inertial}$, as suggested by [12, 5, 35]. Here, the inertial period is

$$T_{inertial} = \frac{2\pi}{2\omega \sin(y)}, \tag{4}$$

where y is the latitudinal position of the drifter and $\omega = 7.27 * 10^{-5}\frac{\text{rad}}{\text{s}}$ is the rotation rate of the Earth.
At mid-latitudes, inertial oscillations have time-scales of 1-2 days, whereas the dominant period of submesoscale and mesoscale eddy motion is above 5 days [40]. The characteristic time of submesoscale and mesoscale features thus greatly exceeds the inertial period. Hence, the anticyclonic looping arising from high-frequency diurnal inertial oscillations does not influence the relative dispersion of drifters in the submesoscale and mesoscale regime [5].

3 Methods

The drifter trajectories, $\mathbf{x}(t)$, satisfy the differential equation

$$\dot{\mathbf{x}}(t) = \mathbf{v}(\mathbf{x}, t), \qquad \mathbf{x}(t) \in U \subset \mathbb{R}^2, \qquad t \in [t_0, t_N], \qquad \mathbf{x}(t_0) = \mathbf{x}_0. \tag{5}$$

Here $\mathbf{x}$ is a position variable, t is a time variable and $\mathbf{v}(\mathbf{x}(t), t)$ is the underlying true surface ocean velocity field captured by the drifter data. Open-ocean mesoscale features are captured by satellite altimetry data [8]. In coastal areas, however, the velocity $\mathbf{v}(\mathbf{x}, t)$ of the drifters generally differs from the geostrophic velocity component $\mathbf{v}_g(\mathbf{x}, t)$ computed from AVISO due to coastal influences and windage [3]. Features derived from drifter trajectories, therefore, generally differ from those obtained from ocean geostrophic velocities, especially in coastal areas.

3.1 Trajectory rotation average

As already noted in the Introduction, LCSs of the velocity field are material sets and hence their existence and location are objective, i.e., indifferent to the observer. All traditionally analyzed features of trajectory data (such as length, curvature, velocity, acceleration and looping) are, in contrast, observer-dependent and hence do not allow for a self-consistent identification of LCSs. To this end, [25, 26] developed several quasi-objective diagnostic tools for single trajectories that do approximate objective features of trajectories in frames verifying certain conditions. Inspired by the slowly varying nature of geophysical flow data sets, we restrict our discussion to a family of frames related to each other via slowly varying (or adiabatic) Euclidean coordinate transformations

$$\mathbf{x} = \mathbf{Q}(t)\mathbf{y} + \mathbf{b}(t), \quad |\dot{\mathbf{Q}}|, |\dot{\mathbf{b}}| \ll 1. \tag{6}$$

Under such slowly varying frame changes, the velocity $\tilde{\mathbf{v}}$ transforms approximately as an objective vector, i.e,

$$\tilde{\mathbf{v}} = \mathbf{Q}^T(\mathbf{v} - \dot{\mathbf{Q}}^T\mathbf{y} - \dot{\mathbf{b}}) \sim \mathbf{Q}^T\mathbf{v}, \tag{7}$$

where $\mathbf{v}$ and $\tilde{\mathbf{v}}$, respectively, denote the velocity in the original and in the slowly varying frame. We refer to a quantity as adiabatically quasi-objective if in all frames related to each other via eq. 6, the quantity approximates the same objective quantity as long as the frames satisfy a set of conditions. Those conditions are specific to the quantity of interest (see, eq. 9 and eq. 10)

We apply one of these single-trajectory rotation diagnostics here, for the first time, to actual sparse drifter data. Similarly to [25], we consider discretized drifter trajectories $\{\mathbf{x}(t_i)\}_{i=0}^N$ satisfying eq.(5). As shown in [25, 26], the trajectory rotation average

$$\overline{\mathrm{TRA}}_{\mathrm{t_0}}^{\mathrm{t_N}}(\mathbf{x}_0) = \frac{1}{t_N - t_0}\sum_{i=0}^{N-1}\cos^{-1}\frac{\langle \dot{\mathbf{x}}(t_i), \dot{\mathbf{x}}(t_{i+1})\rangle}{|\dot{\mathbf{x}}(t_i)||\dot{\mathbf{x}}(t_{i+1})|} \tag{8}$$

approximates a time-averaged trajectory rotation relative to the overall rotation in the flow over the time-interval $[t_0, t_N]$, in a frame of reference satisfying

$$|\frac{\partial \mathbf{v}(\mathbf{x}(t), t)}{\partial t}| \ll |\ddot{\mathbf{x}}(t)|. \tag{9}$$

Condition 9 expresses the requirement that Lagrangian time scales dominate Eulerian time scales. This requirement has been numerically verified for the AVISO data set in [26] and confirmed in several experimental studies on surface drifters [11, 59, 32]. As a second condition for $\overline{\mathrm{TRA}}_{\mathrm{t_0}}^{\mathrm{t_N}}(\mathbf{x}_0)$ to be an adiabatically quasi-objective scalar field (i.e.

approximate an objective scalar field), the Lagrangian acceleration must dominate the angular acceleration of the trajectory induced by the spatial mean vorticity

$$|\overline{\omega}(t) \times \frac{\dot{\mathbf{x}}(t)}{|\dot{\mathbf{x}}(t)|}| \ll |\frac{d}{dt}\frac{\dot{\mathbf{x}}(t)}{|\dot{\mathbf{x}}(t)|}|. \tag{10}$$

This assumption has been found to hold on large enough domains in the ocean [23, 1, 6, 25].

We associate to the trajectory $\mathbf{x}(t;\mathbf{x}_0,t_0) := \mathbf{x}(t)$ over the time-interval $[t_0, t_N]$ its corresponding $\overline{\mathrm{TRA}}_{\mathrm{t_0}}^{\mathrm{t_N}}(\mathbf{x}_0)$ value. Reconstructing the $\overline{\mathrm{TRA}}_{\mathrm{t_0}}^{\mathrm{t_N}}(\mathbf{x}_0)$-field from sparse drifter trajectories via scattered interpolation allows visualization of vortical flow structures. The only parameter involved in the reconstruction of the $\overline{\mathrm{TRA}}_{\mathrm{t_0}}^{\mathrm{t_N}}(\mathbf{x}_0)$-field is the choice of the scattered interpolation method. As vortices tend to be elliptic geometric objects, we use linear radial basis function interpolation which favors such structures. We then apply a spatial average filter of size $(0.25° \times 0.25°)$ in order to suppress noise but still retain small-scale features. The size of the spatial filter is equivalent to the resolution of the AVISO data set. Local maxima in the $\overline{\mathrm{TRA}}_{\mathrm{t_0}}^{\mathrm{t_N}}(\mathbf{x}_0)$-field mark areas of high material rotation and hence indicate underlying rotational flow features.

3.2 Trajectory length

The trajectory length (also commonly referred to as M-function) is a single-trajectory Lagrangian diagnostic, that is applicable to sparse sets of fluid trajectories [39, 37]. As pointed out by [54, 55], this diagnostic is non-objective and has no direct relation to material stretching or rotation. It is nevertheless simple to compute as the arc-length of a trajectory $\mathbf{x}(t)$ over the time-interval $[t_0, t_N]$ starting at $\mathbf{x}_0$ is

$$\mathrm{M}_{\mathrm{t_0}}^{\mathrm{t_N}}(\mathbf{x}_0) = \sum_{i=0}^{N-1} |\dot{\mathbf{x}}(t_i)|\Delta t_i, \quad \text{with } \Delta t_i = |t_{i+1} - t_i| \tag{11}$$

In an attempt to visualize elliptic LCSs from a set of sparse drifter data, we reconstruct $\mathrm{M}_{\mathrm{t_0}}^{\mathrm{t_N}}(\mathbf{x}_0)$ over a broader domain using linear radial basis function coupled with a spatial average filter of size $(0.25° \times 0.25°)$ as done for the $\overline{\mathrm{TRA}}_{\mathrm{t_0}}^{\mathrm{t_N}}(\mathbf{x}_0)$. The references of $\mathrm{M}_{\mathrm{t_0}}^{\mathrm{t_N}}(\mathbf{x}_0)$ suggest that dynamical regions in the flow are separated by abrupt variations of $\mathrm{M}_{\mathrm{t_0}}^{\mathrm{t_N}}(\mathbf{x}_0)$. Specifically, oceanic eddies are signaled by local minima surrounded by a dense set of closed contours of $\mathrm{M}_{\mathrm{t_0}}^{\mathrm{t_N}}(\mathbf{x}_0)$.

3.3 Lagrangian spin

Considering looping trajectories as footprints of coherent Lagrangian eddies, [64, 18, 12, 35] extract looping drifter segments using the Lagrangian spin

$$\Omega(t_i) = \frac{\langle \mathbf{e}_z, \dot{\mathbf{x}}_{\mathbf{eddy}}(t_i) \times \ddot{\mathbf{x}}_{\mathbf{eddy}}(t_i)\rangle}{\frac{1}{2}|\dot{\mathbf{x}}_{\mathbf{eddy}}(t_i)|^2}, \tag{12}$$

first introduced in [57]. The term $\dot{\mathbf{x}}_{\mathbf{eddy}}(t_i)$ denotes the eddy velocity and $\mathbf{e}_z = (0,0,1)^T$. In [18], the eddy velocity $\dot{\mathbf{x}}_{\mathbf{eddy}}(t_i)$ was obtained by removing the background large scale flow $\mathbf{u}_{\mathbf{avg}}$ from the velocity $\dot{\mathbf{x}}(t_i)$ of the drifters:

$$\dot{\mathbf{x}}_{\mathbf{eddy}}(t_i) = \dot{\mathbf{x}}(t_i) - \mathbf{u}_{\mathbf{avg}} \tag{13}$$

However, recent work points out that removing the background mean current $\mathbf{u}_{\mathbf{avg}}$ results in misidentification of looper segments [35]. Hence, we assume that the drifter velocity is dominated be the eddy fluctuating component rather than the large scale background flow:

$$\dot{\mathbf{x}}_{\mathbf{eddy}}(t_i) \sim \dot{\mathbf{x}}(t_i). \tag{14}$$

The Lagrangian spin Ω quantifies the rotation of the velocity vector and is physically related to the vorticity. Evaluating eq. 12 along a Lagrangian particle trajectory provides an overall measure of rotation within a time series over the time-interval $[t_0, t_N]$. Looping segments of a trajectory are characterized as intervals between zero crossings of Ω. The duration of each segment of sustained positive or negative Ω is referred to as the persistence. For each segment, we define the period P:

$$P = \frac{2\pi}{|\Omega^*|}, \tag{15}$$

where $|\Omega^*|$ is the absolute value of the median of Ω over the segment. The time-series of the Lagrangian spin parameter is smoothed using a 3-day median filter in order to suppress noisy observations, as suggested by [35]. Looping segments are defined as trajectory intervals where the persistence exceeds the ad-hoc chosen threshold value of $2P$, as proposed in [35]. Hence, the looping trajectory segments inherently depend on the choice of the minimum looping period.

3.4 Lagrangian averaged vorticity deviation

Similar to the $\overline{\text{TRA}}$, the Lagrangian averaged vorticity deviation (LAVD) characterizes the local material rotation in the flow relative to the overall rotation induced by the spatial mean of the vorticity [24]. Computing the LAVD value for a trajectory $\mathbf{x}(t; \mathbf{x}_0, t_0)$ over the time-interval $[t_0, t_N]$, requires evaluating the vorticity

$$\omega(\mathbf{x}(t), t) = \nabla \times \mathbf{v}(\mathbf{x}(t), t)$$

along the particle trajectories:

$$\text{LAVD}_{t_0}^{t_N}(\mathbf{x}_0) = \frac{1}{t_N - t_0} \int_{t_0}^{t_N} |\omega(\mathbf{x}(s), s) - \overline{\omega}(s)| ds, \tag{16}$$

where $\overline{\omega}(t)$ denotes the spatially averaged vorticity at time t. Therefore, even though the LAVD is a quantity associated to a single trajectory, its computation requires the knowledge of the velocity field over a large enough domain. This renders the LAVD method inapplicable to sparse drifter data, even though it has been used to visualize and extract vortices from gridded ocean velocity data sets [24, 1, 7]. Local maxima in the LAVD-field surrounded by nested closed and nearly convex level curves highlight elliptic LCSs. In this work, we apply the LAVD method to the AVISO data and compare the eddies obtained in this way with those revealed by the $\overline{\text{TRA}}$ from drifter data.

4 Results

4.1 Grand LAgrangian Deployment (GLAD)

Drifters released in the GLAD experiment have mostly been used to study dispersion in the ocean over a range of scales [48, 5, 40]. Furthermore, refs. [47] and [46] found correlation between the evolution of the drifters and nearby attracting LCSs extracted from the geostrophic velocity field. Specifically, drifter behavior agreed with the *tiger tail* pattern inferred from the chlorophyll distribution shown in Fig. 1. A chlorophyll plume extended over more than 100 kilometres from the outlet of the Mississippi river into the open sea and coincided with an attracting LCS [46]. The attracting LCS (continuous black line in Fig. 1) is computed from the geostrophic velocity field $\mathbf{v_g}$ using backward trajectories over the time-interval $[222 \text{ doy}, 229 \text{ doy}]$ according to [14]. Drifters in the proximity of the tip of the tiger tail organized themselves into long filaments along the attracting LCS. Some of the drifters (in red) additionally exhibited some degree of clustering, suggesting the presence of an elliptic LCS close to the chlorophyll front.

Here we seek to visualize vortices by reconstructing the $\overline{\text{TRA}}$-field from drifter data over the interval $[222 \text{ doy}, 229 \text{ doy}]$ using linear radial basis function interpolation. The $\overline{\text{TRA}}$, shown in Fig. 2, is plotted with respect to the final drifter positions at time $t = 229$ doy. This plot reveals multiple rotational features marked by local maxima of the $\overline{\text{TRA}}$ surrounded by a dense set of closed and almost convex contours. For comparison, we include three further Lagrangian eddy diagnostics: the LAVD computed from geostrophic velocity currents, the trajectory length (also called M-function) and the Lagrangian spin computed from drifter data.

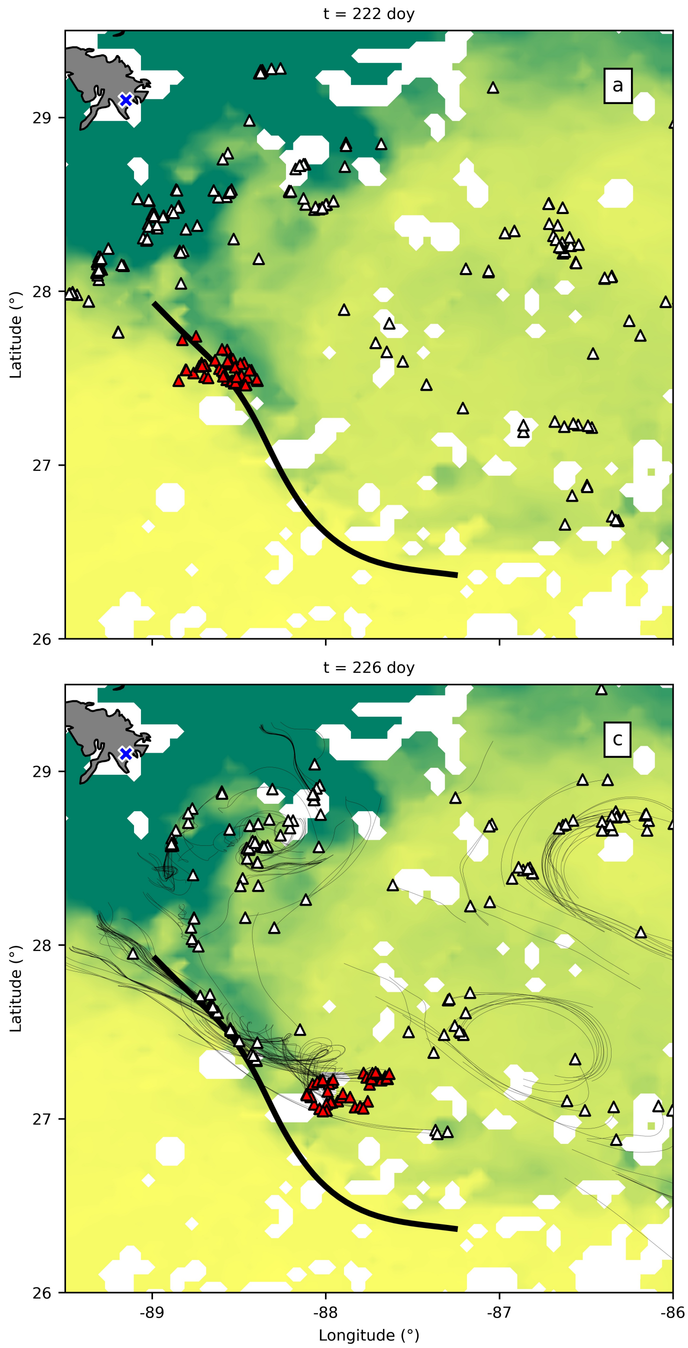

Figure 1: Evolution of GLAD-drifters overlayed on 8-day composite chlorophyll-a concentration (12 August, 2012). Most drifters (white triangles) formed a long filament along the chlorophyll plume (and attracting LCS) extending deep into the Gulf of Mexico. Drifters additionally forming a visible tight cluster are colored in red. The blue cross denotes the outlet of the Mississippi river. The black line corresponds to the attracting LCS.

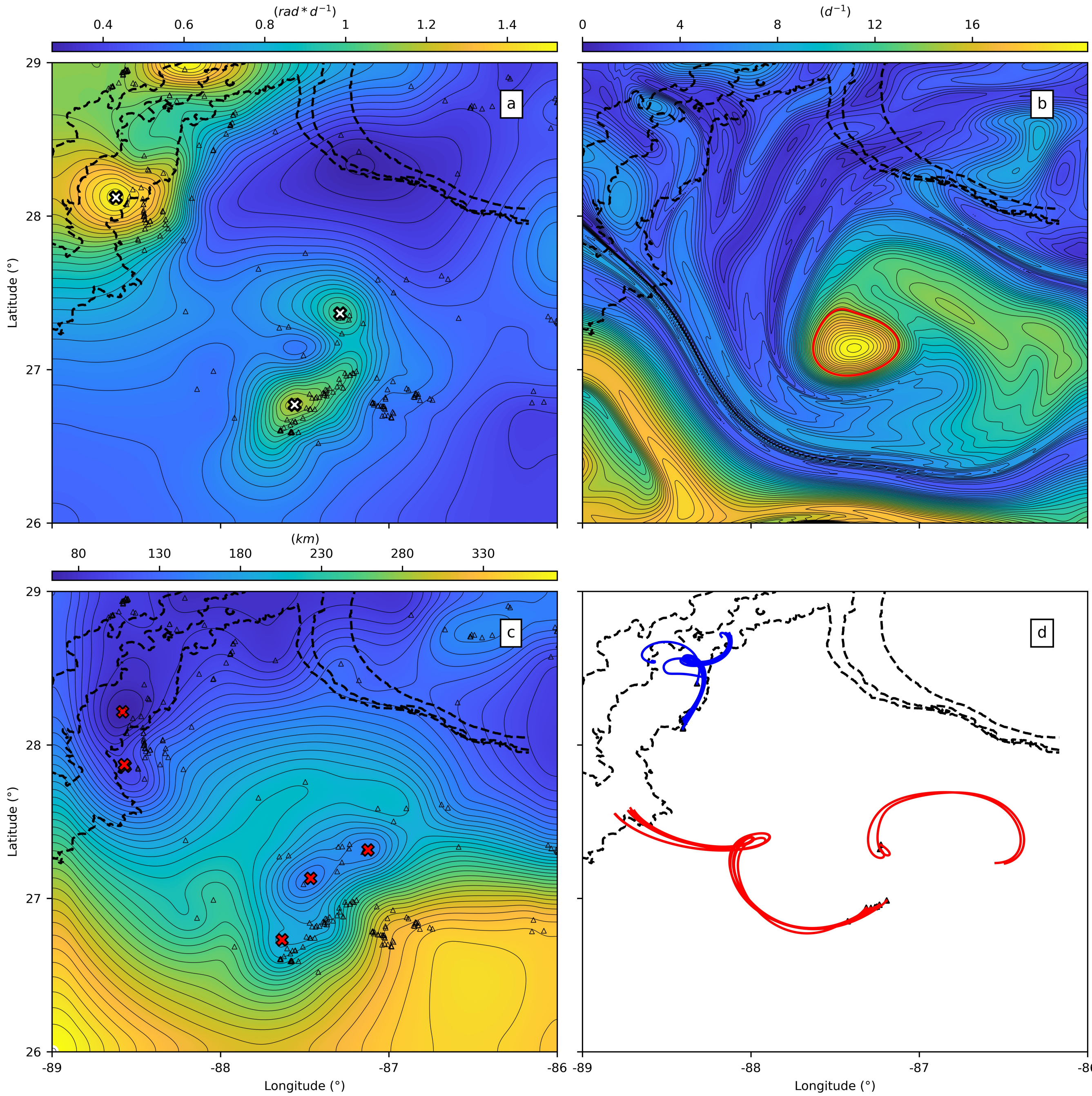

Figure 2: Different material eddy diagnostics computed from the GLAD data set or the AVISO data set. The dashed black lines correspond to the isobaths (-1000 m, -1500 m, -2000 m) and highlight the coastal area. (a) Reconstructed $\overline{\mathrm{TRA}}_{222}^{229}$-field plotted with respect to the position of the drifters at time $t = 229$ doy. White crosses indicate local maxima. (b) $\mathrm{LAVD}_{222}^{229}$-field computed from AVISO plotted at time $t = 229$ doy. The closed red curve denotes the eddy boundary extracted from the $\mathrm{LAVD}_{222}^{229}$-field. (c) Reconstructed M_{222}^{229}-field plotted with respect to the position of the drifters at time $t = 229$ doy. Red crosses indicate local minima. (d) Cyclonic (red) and anticyclonic (blue) loopers.

4.1.1 Coastal area

We start by focusing on the area at the outlet of the Mississippi river on the continental shelf. Coastal flows are regions of intense mixing [3], often characterized by high potential vorticity and strong horizontal shear, which are responsible for the formation of small-scale eddies [60, 61]. Anticyclonic looping segments extracted from the Lagrangian spin parameter, confirm the presence of small-scale vortices at the outlet of the Mississippi river (Fig. 2d). Evidence for the existence of submesoscale elliptic features and strong mixing areas on the continental shelf is also found in the $\overline{\mathrm{TRA}}$ (Fig. 2a). Vortices are revealed in the $\overline{\mathrm{TRA}}$ as local maxima surrounded by a dense set of closed curves indicating abrupt spatial variations. The local maximum of the $\overline{\mathrm{TRA}}$ at $(88.6°W, 28.1°N)$ is surrounded by a dense set of closed contours, thereby indicating high spatial gradients in the $\overline{\mathrm{TRA}}$-field. Close to the vortical flow features identified by the $\overline{\mathrm{TRA}}$ in the coastal area, the M-function displays two local minima, respectively at $(88.6°W, 28.2°N)$ and $(88.5°W, 27.8°N)$ (Fig. 2c). Similarly to the $\overline{\mathrm{TRA}}$ and the Lagrangian spin parameter, the M-function also indicates the existence of coastal eddies. However, compared to the $\overline{\mathrm{TRA}}$, which displays a unique local maximum surrounded by a dense set of closed and convex curves, the M-function displays multiple local minima surrounded by sparse level sets, thereby indicating a flat structure with no abrupt variations.

The LAVD-field displays no distinguished features close to the outlet of the Mississippi river (Fig. 2b). Eddy boundaries are viewed as outermost (almost) convex contours around a local maximum in the LAVD-field [24]. Passing from the LAVD-field to a discrete set of (closed) curves requires specifying two parameters: the minimum length l_{min} of the perimeter of the eddy and the convexity deficiency c_d. The convexity deficiency is

$$c_d = \frac{|A_{contour} - A_{contour,convex}|}{A_{contour}}, \tag{17}$$

where $A_{contour}$ is the area enclosed by the closed contour and $A_{contour,convex}$ is the area enclosed by the convex hull of the closed contour. Similarly to [24], we set $c_d = 10^{-3}$. As a threshold for the perimeter of the eddy l_{min}, we select $l_{min} = 2\pi r$, with $r = 25km$ ($\sim 0.25°$). This corresponds to the minimal length scales that can reliably be resolved by the AVISO data set with a spatial resolution of $(0.25° \times 0.25°)$. The LAVD does not reveal the presence of coastal eddies (Fig. 2b). We attribute the mismatch between the LAVD and the above discussed drifter-based diagnostics to the insufficient resolution of the underlying ocean surface velocity close to the outlet of the Mississippi river by the AVISO data set. Hence, in coastal areas, the drifter-based $\overline{\mathrm{TRA}}$ diagnostic captures the flow dynamics with higher detail than the AVISO-based LAVD.

4.1.2 Open sea

The $\overline{\mathrm{TRA}}$ highlights another family of elliptic LCSs close to the chlorophyll plume extending from the outlet of the Mississippi river to the open ocean (Fig. 2a). The two local maxima associated to the elliptic LCSs are respectively located at $(87.5°W, 26.8°N)$ and $(87.3°W, 27.4°N)$. Due to the close proximity of these extrema, it is, however, a-priori unclear whether they highlight two separate eddies or whether they are part of the same mesoscale eddy. The cyclonic looping segments confirm the presence of vortical flow features in this area (red trajectories in Fig. 2d), but do not specifically highlight eddy boundaries. Inspection of the cyclonic trajectories suggests that they are originally part of two distinct eddies as they come from two separate regions. Extracting looping trajectory segments from the time-series of the Lagrangian spin is a powerful methodology. However, discriminating between loopers and non-loopers requires an ad-hoc choice of the minimum sustained looping period of a trajectory. Contrarily, the $\overline{\mathrm{TRA}}$ retains all trajectory information and allows visualization of vortical flow structures from sparse drifter data using a scalar diagnostic.

The investigated elliptic LCSs highlighted by the $\overline{\mathrm{TRA}}$ and the Lagrangian spin are also visible in the LAVD, which displays a nearly convex vortical flow feature (closed red curve in Fig. 2b). Compared to the $\overline{\mathrm{TRA}}$, however, which indicates two separate, albeit closely located local maxima, the LAVD computation clearly reveals a single mesoscale eddy.

In contrast to the aforementioned methods, the features resulting from the trajectory length diagnostic are far less pronounced (Fig. 2c). It displays multiple local minima, which are only partially correlated with the eddies suggested by the other methods. Furthermore, local minima in the M-function are not surrounded by a dense set of closed contours. Hence, extracting eddy-related features from the M-function is challenging as there exist no distinguishable sharp and closed boundaries surrounding local minima.

4.1.3 Eddy dynamics

In order to investigate the formation and evolution of the elliptic LCSs inferred from the drifter-based $\overline{\text{TRA}}$, we proceed by quasi-materially advecting the $\overline{\text{TRA}}$ distribution over the time-interval $[222\text{ doy}, 229\text{ doy}]$ (Fig. 3). True material advection would require a spatiotemporally well-resolved velocity field. In our setting, however, the velocity field is only sparsely known and hence the advected structures are inherently non-material: At every time step, the $\overline{\text{TRA}}$-field must be approximated from the current drifter distribution. Nevertheless, the $\overline{\text{TRA}}$-distribution approximates a materially advected frame-indifferent scalar field along drifter trajectories. The closed white curves in Fig. 3 indicate eddy boundaries extracted from the $\overline{\text{TRA}}$ using the algorithm described in Appendix A. The red closed curve denotes the truly materially advected vortex boundary extracted from the LAVD at time $t = 229$.

The $\overline{\text{TRA}}$-based eddy extraction algorithm requires finding convex closed curves surrounding one or multiple local maxima in the $\overline{\text{TRA}}$-field satisfying a set of conditions (see Appendix A for further details). There are two parameters involved here: the minimum number of drifters n_d required to be inside the eddy and the minimum allowed local maximum $\overline{\text{TRA}}_{\text{loc,max}}$. In the following example, we set $\mathrm{n}_d = 2$ as we expect multiple drifters to be part of the same eddy and $\overline{\text{TRA}}_{\text{loc,max}} = 0.5\overline{\text{TRA}}_{\text{max}}$, where $\overline{\text{TRA}}_{\text{max}}$ is the global maximum of the $\overline{\text{TRA}}$ in the chosen domain. The LAVD-based eddy at $t = 229$ doy is materially advected using the geostrophic velocity $\mathbf{v}_g(\mathbf{x}, t)$, whereas the eddy boundaries inferred from the drifter-based $\overline{\text{TRA}}$ are quasi-materially advected along drifter trajectories.

At $t = 222$ doy, the $\overline{\text{TRA}}$ suggests the presence of several small-scale vortices at the outlet of the Mississippi river and at open sea (see Fig. 3a). The submesoscale eddies close to the outlet of the Mississippi river remain trapped in coastal areas and eventually merge into a larger vortical flow feature. Over the time-interval $[222\text{ doy}, 226\text{ doy}]$, the LAVD-based eddy does not coincide with any of the eddies inferred from the $\overline{\text{TRA}}$ (Fig. 3a-d). The white eddy initially located at approximately $(88.5°W, 27.5°N)$ is associated to the clustered red drifters identified in Fig. 1, thereby confirming the existence of the submesoscale eddy along the chlorophyll front. This agrees with the observation put forward in [47, 46]. The eddy develops along the attracting LCS and then slowly detaches away from the oceanic front (Fig. 3a-f). Drifters are thereby coherently transported from the coastline into the open sea. The drifter-based elliptic LCS evolving along the AVISO-based attracting LCS eventually merges with the submesoscale eddy originally located at $(86.5°W, 27.25°N)$ to form a larger mesoscale eddy at $t = 228$doy (Fig. 3g). Hence, vortical flow structures generated along oceanic fronts represent a possible transport route for particles as they can carry material over long distances away from the coastline into the open sea. We point out that intersections between attracting and elliptic LCS (such as at $t = 222$doy) are physically inconsistent as they would imply contradicting material response. We attribute this inconsistency to the fact that the attracting LCS is computed from $\mathbf{v_g}(\mathbf{x}, t)$ whereas the white elliptic LCSs are computed from drifter velocities. Furthermore, the attracting LCS is assumed to be stationary (i.e. it is not materially advected as done for the elliptic LCS as this would go beyond the scope of this paper).

Towards the end of the advection process, the LAVD-based elliptic LCS (red curve in Fig. 3h) approximates the mesoscale eddy inferred from the $\overline{\text{TRA}}$ (white curve centered at approximately $(87.5°W, 27°N)$ in Fig. 3h). The formation and evolution of the eddy, however, is clearly different. The red eddy shows no degree of filamentation and remains coherent over the full time-interval. The white eddy results from the vortex merger between two smaller eddies and is significantly larger than the red eddy. At $t = 229$ doy the circumference of the $\overline{\text{TRA}}$-based white eddy and the $\overline{\text{LAVD}}$-based red eddy is respectively $298.5km$ and $152km$. As the LAVD-based eddy is a purely materially advected closed curve, it can neither split nor merge with any other materially advected curve. Hence, by construction, the LAVD is unable to capture vortex mergers. In contrast, the quasi-materially advected, $\overline{\text{TRA}}$-based eddies can merge into larger eddies. This follows because the computation of the eddy boundary from the $\overline{\text{TRA}}$-field is independently carried out at each time step.

Kinetic energy (KE) is frequently seen as a footprint of large-scale coherent motion in the ocean [51, 34, 35]. The

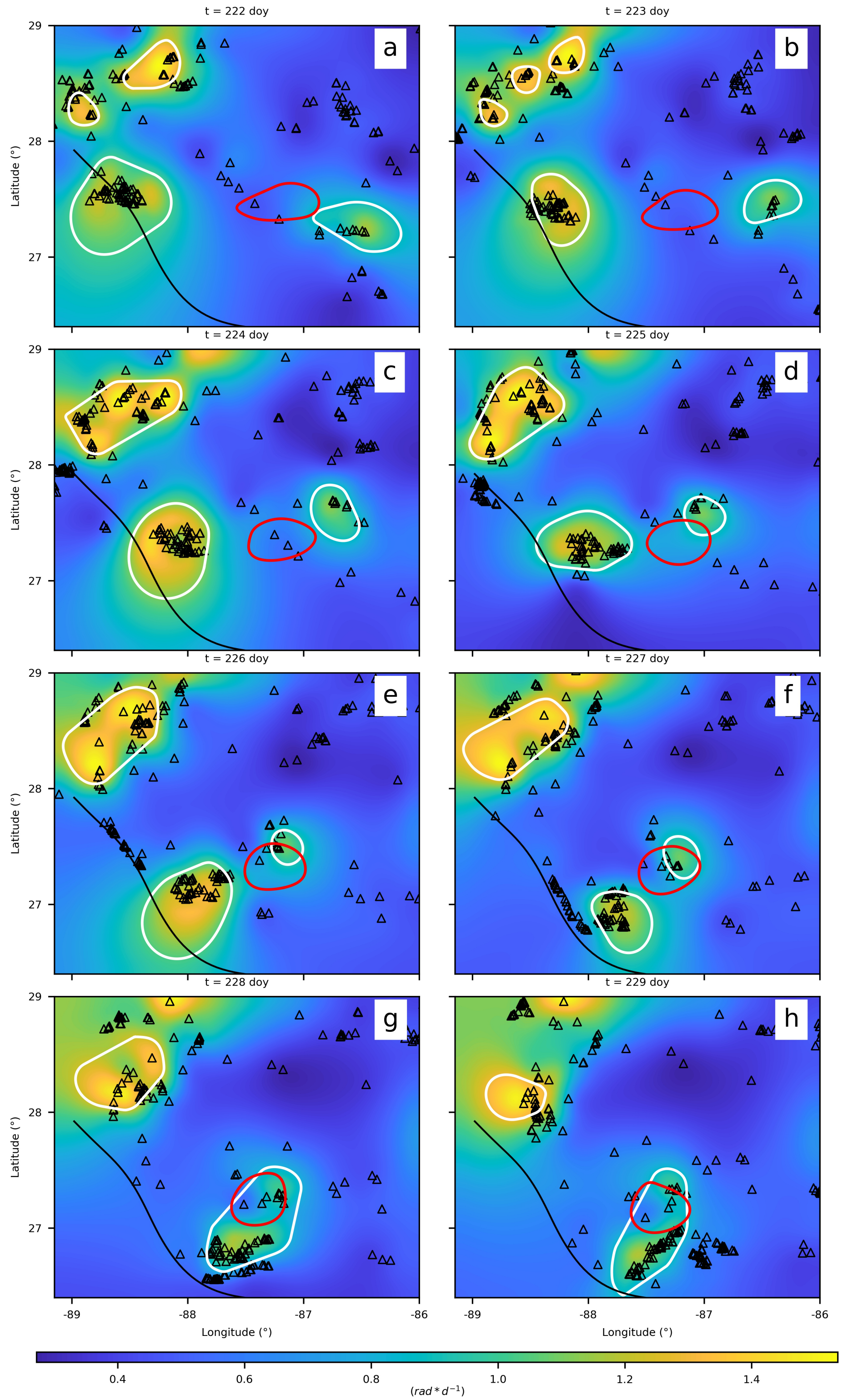

Figure 3: Quasi materially advected $\overline{\mathrm{TRA}}_{222}^{229}$ for the GLAD data set. The black line denotes the AVISO-based attracting LCS. Closed white curves display eddy boundaries extracted from the drifter-based $\overline{\mathrm{TRA}}$ using the algorithm described in Appendix A. Closed red curves indicate eddy boundaries obtained from the AVISO-based LAVD computation. Triangles indicate the positions of the drifters at time t.

averaged KE associated to a trajectory $\mathbf{x}(t)$ over the time-interval $[t_0, t_N]$ starting at $\mathbf{x}_0$ is

$$\overline{\mathrm{KE}}_{\mathrm{t_0}}^{\mathrm{t_N}}(\mathbf{x}_0) = \frac{1}{2|t_N - t_0|} \sum_{i=0}^{N} |\dot{\mathbf{x}}(t_i)|^2 \Delta t_i, \quad \text{with } \Delta t_i = |t_{i+1} - t_i|. \tag{18}$$

$\overline{\mathrm{KE}}$ is a non-objective Lagrangian single-trajectory diagnostics, which bears similarities to the trajectory length diagnostic introduced in sec. 3.2. It is often used to visualize energetically dominant flow structures both from AVISO [36] and drifter data [35]. The AVISO-based $\overline{\mathrm{KE}}$-field is derived from artificial Lagrangian particle trajectories computed from the geostrophic velocity field $\mathbf{v_g}(\mathbf{x}, t)$ in the region of interest (Fig. 4b). It displays a front-like feature coinciding with the attracting LCS responsible for the transport drifters from the outlet of the Mississippi river into the open sea. The drifter-based $\overline{\mathrm{KE}}$-field is reconstructed from sparse drifter data as already done for the M-function and the $\overline{\mathrm{TRA}}$ and shows a front-like feature reminiscent of the front visible in the AVISO-based $\overline{\mathrm{KE}}$ (Fig. 4a). The weakly spiraling feature in the AVISO-based $\overline{\mathrm{KE}}$-field is associated to the mesoscale elliptic LCSs. Overall, however, both methodologies fail to clearly highlight the oceanic eddies detected from $\overline{\mathrm{TRA}}$ and LAVD. Hence, although frequently linked to coherent eddy motions, we conclude that the kinetic energy is not directly related to oceanic eddies in the region of interest.

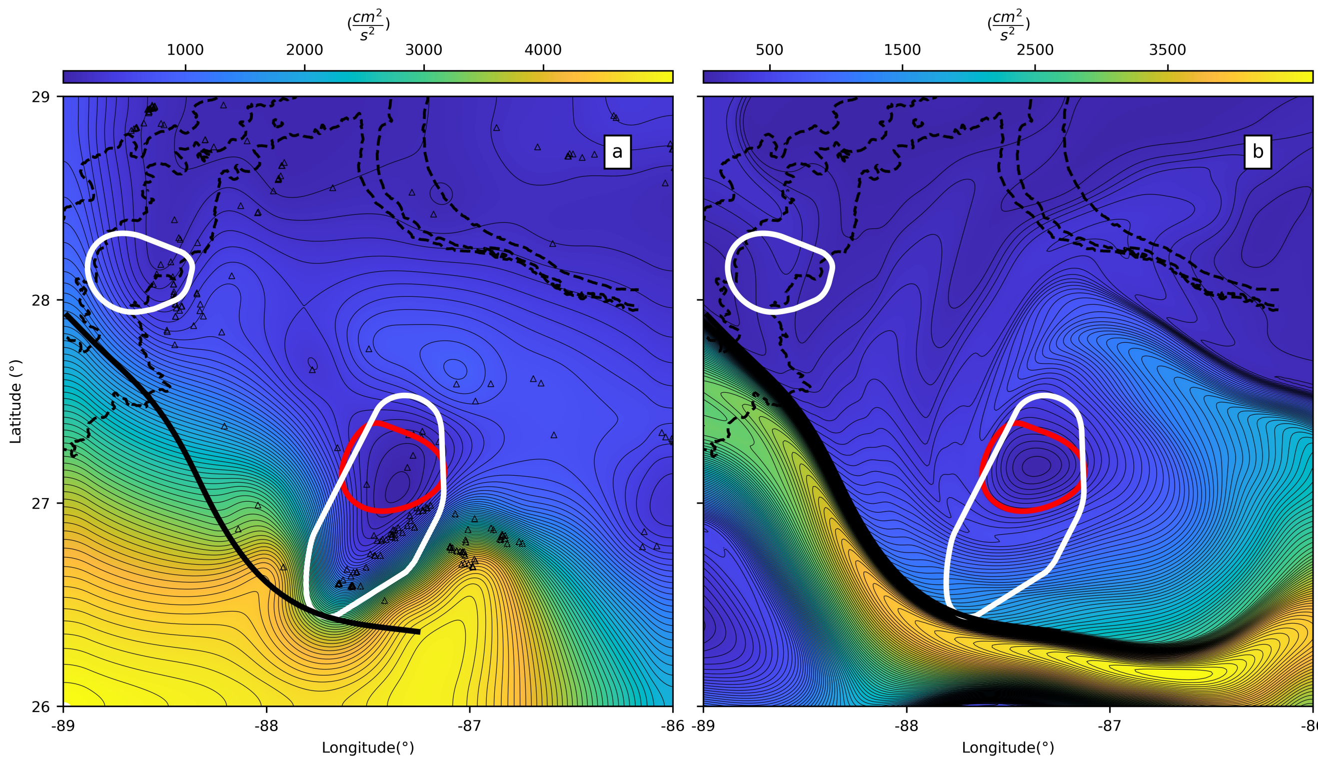

Figure 4: $\overline{\mathrm{KE}}$ evaluated both on GLAD-drifters and on AVISO. The white and red eddies respectively indicate the eddies extracted from the drifter-based $\overline{\mathrm{TRA}}$-field and the AVISO-based LAVD-field. The dashed black lines correspond to the isobaths (-1000 m, -1500 m, -2000 m). The black line denotes the AVISO-based attracting LCS. (a) Reconstructed drifter-based $\overline{\mathrm{KE}}_{222}^{229}$-field plotted with respect to the position of the drifters (triangles) at time $t = 229$ doy. (b) AVISO-based $\overline{\mathrm{KE}}_{222}^{229}$-field at time $t = 229$ doy.

The quasi-material advection of the $\overline{\mathrm{TRA}}$-based eddies sheds new light on the origin and the formation of the mesoscale eddy detected from the AVISO-based LAVD-field. Despite, the minimal amount of data, the $\overline{\text{TRA}}$ reveals eddy dynamics, which are hidden in the AVISO-based LAVD and $\overline{\text{KE}}$.

4.2 Global Drifter Program (GDP)

In our second example, we focus on a set of drifters in the western North-Atlantic. This oceanic region is characterized by a strong and persistent formation of eddies arising from the meanders of the Gulf Stream [27, 50]. On the 4^{th} of October, 2006, a floating sargassum patch was detected by the Medium Resolution Imaging Spectrometer (MERIS) on Envisat. This feature has a spiralling shape that is also visible from satellite-altimetry data [4]. This floating sargassum patch is visualized in Fig. 5b using the Maximum Chlorophyl Index (MCI) [9]. Due to persistent cloud-coverage, such clear snapshots of floating material in the ocean are very rare.

We use the $\overline{\text{TRA}}$ to extract the eddy highlighted by the spiralling sargassum patch described in [4]. We also compute two further single trajectory metrics: the trajectory length diagnostic (Fig. 5c) and the looping segments computed from the Lagrangian spin (Fig. 5d). Instead of evaluating the satellite altimetry based LAVD we include a snapshot of the floating sargassum patch which reveals the presence of an elliptic LCS (Fig. 5b). Similarly to the MCI, the $\overline{\text{TRA}}$ reveals a Lagrangian eddy centered at $(67.6°W, 37.1°N)$. Indeed, this eddy is visible as a distinguished local maximum in the $\overline{\text{TRA}}$-field surrounded by a dense set of closed and convex contours (zoomed inset of Fig. 5a). The white eddy boundary is extracted from the $\overline{\text{TRA}}$ using the algorithm proposed in Appendix A with the same parameters presented in section 4.1.3. The extracted eddy boundary underestimates the size of the sargassum patch, but correctly approximates the location (Fig. 5b). The cyclonic looping exhibited by the two trajectories inside the eddy additionally confirms the presence of an elliptic LCS (Fig. 5d) but does not provide a specific estimate for the eddy boundary. The trajectory length diagnostic shows a nearby maximum (zoomed inset of Fig. 5c), which is inconsistent with the footprint generally envisioned for a coherent eddy in the M-field (see section 3.2).

5 Conclusion

Lagrangian eddies (elliptic LCSs) are material objects responsible for the transport of floating particles over large distances in the ocean. They are, by their definition, frame-indifferent and thus can only be reliably characterized with objective feature extraction methods. The local ocean velocity is most accurately observed from float trajectory data, which, however, is inherently non-objective, representing an inconsistency that available eddy detection methods for sparse trajectories do not address. Those methods typically describe eddies by extracting the looping segments of a trajectory, but their definition of looping depends on the frame of the observer. Furthermore, looping segments of a trajectory are most commonly described by these methods in a statistical sense and hence are not geared towards highlighting individual Lagrangian eddy boundaries with high accuracy.

In this paper, we have proposed to tackle this inconsistency from a dynamical systems perspective by applying the adiabatically quasi-objective $\overline{\text{TRA}}$ diagnostic [25, 26] to sparse drifter data sets. The $\overline{\text{TRA}}$ approximates an objective measure of material rotation in frames satisfying specific conditions that generally hold in the ocean. We have found that vortical flow features are related to regions of high local material rotation. Hence, they can be identified as local maxima in the $\overline{\text{TRA}}$-field. The $\overline{\text{TRA}}$ highlights both submesoscale and mesoscale vortices from sparse drifter data, as demonstrated in our two examples. Furthermore, it also succeeds in characterizing the mixing and stirring processes in coastal flow regions and captures the merger of two originally distinct eddies. Contrary to other single trajectory diagnostics, both the $\overline{\text{TRA}}$ and the LAVD are physically related to the local material rotation in the flow. Compared to the LAVD, which correctly highlights vortical flow features given a sufficiently densely gridded velocity data set, the $\overline{\text{TRA}}$ can be applied to arbitrarily sparse drifter data. Hence, it allows incorporating valuable drifter data into the analysis of oceanic coherent structures in a physically and mathematically justifiable way. This proves to be especially useful in ocean regions, where satellite altimetry data does not unravel the true ocean dynamics.

Importantly, the looper segments extracted from the Lagrangian spin coincide with the features identified in the $\overline{\text{TRA}}$. However, a spaghetti plot of looping trajectory segments does not immediately reveal transport barriers and

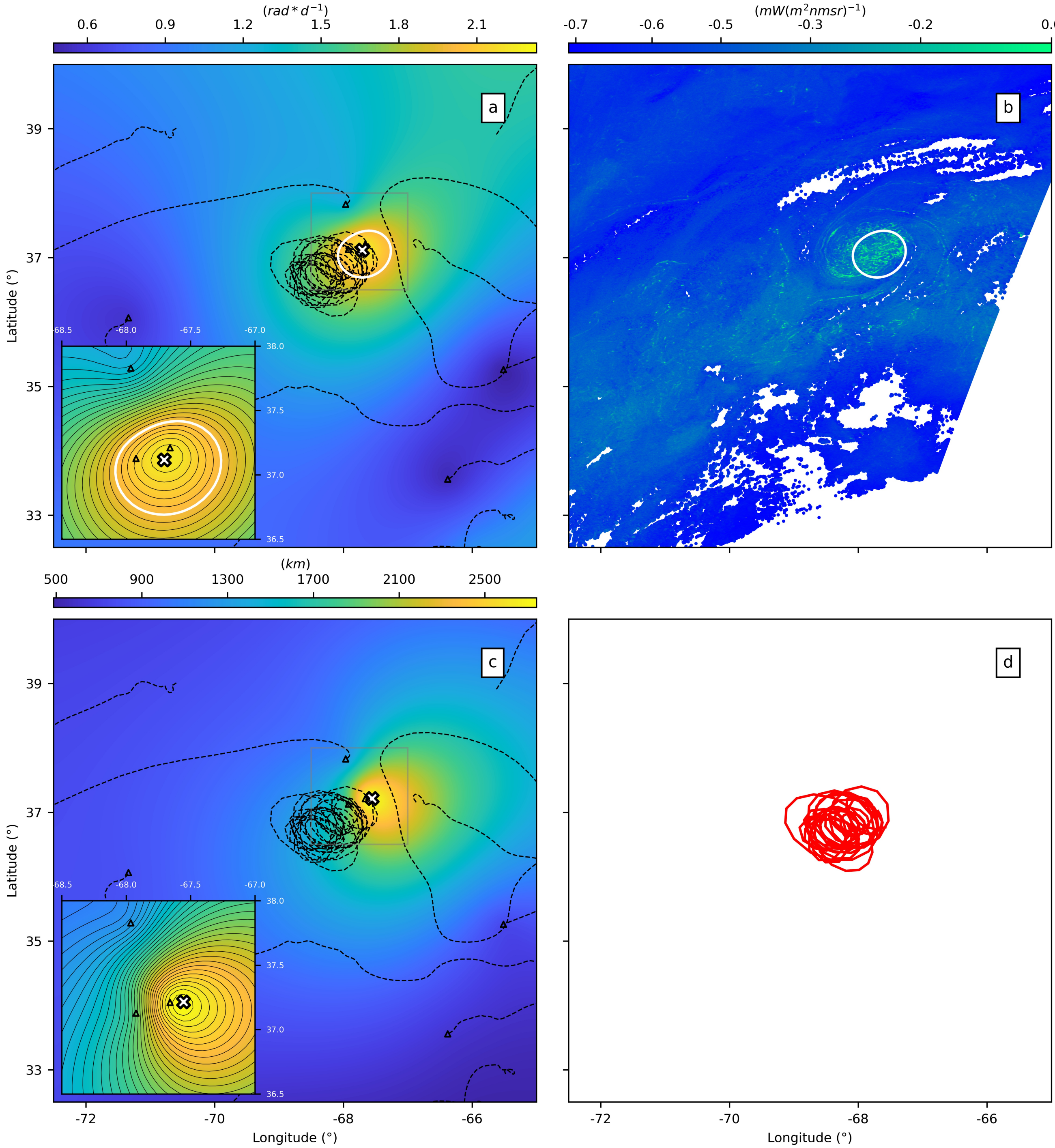

Figure 5: Lagrangian diagnostics evaluated on a subset of the GDP data set. (a) Reconstructed $\overline{\mathrm{TRA}}_{246}^{276}$-field plotted with respect to the position of the drifters (triangles) at time $t = 276$ doy. White cross indicates unique local maximum in the $\overline{\mathrm{TRA}}_{246}^{276}$-field. (b) Eddy boundary superimposed on the floating sargassum concentration inferred from the Maximum Chlorophyl Index (MCI) at $t = 276$ doy. Regions covered by clouds are displayed in white. (c) Reconstructed M_{246}^{276}-field plotted with respect to the position of the drifters (triangles) at time $t = 276$ doy. White cross indicates unique local maximum in the M_{246}^{276}-field. (d) Cyclonic (red) loopers.

eddy boundaries. Furthermore, potentially valuable information is lost when we discard non-looping trajectory segments based on a manually tuned threshold parameter. The trajectory length diagnostic [39, 37] also tended to show either minima or maxima near the material eddies highlighted by the local maxima of the $\overline{\mathrm{TRA}}$-field. This variation in extremum types creates ambiguity in using the trajectory length as a stand-alone indicator in detecting elliptic LCSs from sparse data sets.

Apart from the visual inspection of the reconstructed $\overline{\mathrm{TRA}}$-field, we have additionally presented an algorithm to extract approximate eddy boundaries from sparse drifter data. As vortical flow features are indicated by blobs close to local maxima in the $\overline{\mathrm{TRA}}$-field, the proposed method resembles a blob detection algorithm. Passing from a continuous scalar diagnostic field to a set of closed curves, inevitably requires introducing user-defined parameters. All in all, however, the number of free parameters is comparable to other multi-trajectory Lagrangian eddy detection methods [24, 62]. This is noteworthy as these algorithms were originally designed assuming knowledge of the underlying velocity field.

This work represents one of the first attempts to apply a physically justifiable Lagrangian diagnostic quantity to a sparse set of drifter data. We compared the outcome of several commonly used single particle trajectory diagnostics over dynamically distinct data sets and find that the $\overline{\mathrm{TRA}}$ efficiently characterizes elliptic LCSs. Furthermore, the $\overline{\mathrm{TRA}}$-based Lagrangian vortex detection algorithm developed here shows promise of general applicability to drifter data sets.

A Eddy Boundary Extraction Algorithm

Algorithm 1 Extraction of approximate eddy boundaries from $\overline{\mathrm{TRA}}_{\mathrm{t}_0}^{\mathrm{t}_\mathrm{N}}$-field

Input: Trajectories over the time-interval $[t_0, t_N]$.

1. Reconstruct $\overline{\mathrm{TRA}}_{\mathrm{t}_0}^{\mathrm{t}_\mathrm{N}}$-field at time t using linear radial basis interpolation. It is recommended to additionally filter the resulting $\overline{\mathrm{TRA}}_{\mathrm{t}_0}^{\mathrm{t}_\mathrm{N}}$ using a spatial average filter to reduce noise.
2. Find local maxima of $\overline{\mathrm{TRA}}_{\mathrm{t}_0}^{\mathrm{t}_\mathrm{N}}$ which are above a threshold $\overline{\mathrm{TRA}}_{\mathrm{loc,max}}$.
3. Compute for each closed level set surrounding a local maximum, the averaged $|\nabla\overline{\mathrm{TRA}}_{\mathrm{t}_0}^{\mathrm{t}_\mathrm{N}}|$ along the level set.
4. Find closed level set with the highest averaged $|\nabla\overline{\mathrm{TRA}}_{\mathrm{t}_0}^{\mathrm{t}_\mathrm{N}}|$ which additionally
   (a) has at least one local maximum of $\overline{\mathrm{TRA}}_{\mathrm{t}_0}^{\mathrm{t}_\mathrm{N}}$ in its interior.
   (b) contains at least n_d-trajectories.
5. Take the convex hull of all the selected closed curves.
6. If two or more convex closed curves intersect, then take the union of these curves.
7. Take the convex hull of the resulting closed curves.

Output: Approximate eddy boundaries at time t.

While various eddy extraction algorithms are presented in [65, 21, 23, 58], these methods assume a trajectory density that is generally unavailable for drifter trajectories in the ocean. Here, we propose an algorithm that extracts approximate eddy boundaries from the topology of the reconstructed $\overline{\mathrm{TRA}}$-field. Vortices are then identified by this algorithm as local maxima of the $\overline{\mathrm{TRA}}$-field surrounded by a dense set of closed and convex curves characterized by high spatial gradients.

Passing from a continuous scalar field to a set of discrete closed curves representating eddy boundaries, inevitably requires introducing threshold parameters. There are two main parameters involved in Algorithm 1. The first user-defined quantity aids the identification of the local maxima in the $\overline{\mathrm{TRA}}$-field. As we identify vortical flow features with regions of high $\overline{\mathrm{TRA}}$, local maxima below a predefined threshold $\overline{\mathrm{TRA}}_{\mathrm{loc,max}}$ are neglected. Additionally, we also need to specify the minimum number of drifters n_d inside an eddy. As elliptic LCSs are often observed via a dense clustering of multiple drifters, this parameter is generally set to be greater than 1. The choice of the parameters inevitably influences the number and size of the extracted eddies. By construction, the extracted eddy boundaries are closed convex curves characterized by sharp gradients. They do not necessarily coincide with closed level sets of the $\overline{\mathrm{TRA}}$.

Data Availability

The AVISO geostrophic current velocity product used in this study, "Global Ocean Gridded L4 Sea Surface Heights and Derived Variables Reprocessed, "is freely available and is hosted by the Copernicus Marine Environment Monitoring Service (http://marine.copernicus.eu). The attracting LCS and LAVD computations are done with the software TBarrier. Jupyter notebooks (together with drifter data) implementing the methods described are shared on Github/EncinasBartos. The codes can readily be applied to any sparse trajectory data set.

References

[1] R. Abernathey and G. Haller, "Transport by lagrangian vortices in the eastern pacific," *Journal of Physical Oceanography* **48.3** (2018): 667-685.

[2] R. Abernathey, C. Bladwell, G. Froyland, and K. Sakellariou, "Deep Lagrangian connectivity in the global ocean inferred from Argo floats," *Journal of Physical Oceanography.* (2021)

[3] N. Aksamit, T. Sapsis, G. Haller, "Machine-Learning Mesoscale and Submesoscale Surface Dynamics from Lagrangian Ocean Drifter Trajectories," *Journal of Physical Oceanography*, **50** (2020) 1179–1196.

[4] F. J. Beron-Vera, M.J. Olascoaga, G. Haller, M. Farazmand, J. Triñanes, and Y. Wang, "Dissipative inertial transport patterns near coherent Lagrangian eddies in the ocean," *Chaos: An Interdisciplinary Journal of Nonlinear Science*, **25** (2015), 087412.

[5] F.J. Beron-Vera, and J.H. LaCasce, "Statistics of simulated and observed pair separations in the Gulf of Mexico," *Journal of Physical Oceanography*, **46** (2016), 2183–2199.

[6] F. J. Beron-Vera, A. Hadjighasem, Q. Xia, M.J. Olascoaga, M. J., and G. Haller, "Coherent Lagrangian swirls among submesoscale motions," *Proceedings of the National Academy of Sciences*, **(116)** (2019) 18251–18256.

[7] F. J. Beron-Vera and P. Miron, "A minimal Maxey-Riley model for the drift of Sargassum rafts," *Journal of Fluid Mechanics*, **904** (2020).

[8] M. Berta, A. Griffa, M.G. Magaldi, T.M. Özgökmen, A.C. Poje, A.C. Haza and M.J. Olascoaga, "Improved surface velocity and trajectory estimates in the Gulf of Mexico from blended satellite altimetry and drifter data.," *Journal of Atmospheric and Oceanic Technology*, **(10)**, (2015) 1880-1901.

[9] C. E. Binding, T.A. Greenberg, R.P. Bukata, "The MERIS maximum chlorophyll index; its merits and limitations for inland water algal bloom monitoring," *Journal of Great Lakes Research*, **39** (2013), 100–107.

[10] D.B. Chelton, G.S. Michael, M.S. Roger, and R. A. de Szoeke, "Global observations of large oceanic eddies," *Geophysical Research Letters* **34** (2007).

[11] R. E. Davis, "Drifter observations of coastal surface currents during CODE: The method and descriptive view," *Journal of Geophysical Research: Oceans*, **90** (1985), 4741–4755.

[12] C. Dong, Y. Liu, R. Lumpkin, M. Lankhorst, D. Chen, J.C. McWilliams and Y. Guan, "A scheme to identify loops from trajectories of oceanic surface drifters: An application in the Kuroshio Extension region," *Journal of Atmospheric and Oceanic Technology*, **28** (2011), 1167-1176.

[13] J. H. Faghmous, I. Frenger, Y. Yao, R. Warmka, A. Lindell and V. Kumar, "A daily global mesoscale ocean eddy dataset from satellite altimetry," *Scientific data*, **2** (2015), 1-16.

[14] M. Farazmand and G. Haller, "Computing Lagrangian coherent structures from their variational theory," *Chaos: An Interdisciplinary Journal of Nonlinear Science*, **22(1)** (2012), 013128.

[15] G. Froyland, R.M. Stuart and E. van Sebille, "How well-connected is the surface of the global ocean?" *Chaos: An Interdisciplinary Journal of Nonlinear Science*, **24** (2014), 033126.

[16] G. Froyland and K. Padberg-Gehle, "A rough-and-ready cluster-based approach for extracting finite-time coherent sets from sparse and incomplete trajectory data," *Chaos: An Interdisciplinary Journal of Nonlinear Science*, **25** (2015), 087406.

[17] A. Griffa, "Applications of stochastic particle models to oceanographic problems," *Stochastic modelling in physical oceanography* (pp. 113–140) (1996).

[18] A. Griffa, R. Lumpkin, and M.Veneziani, "Cyclonic and anticyclonic motion in the upper ocean, " *Geophysical Research Letters*, **35** (2008).

[19] J. Gula, M.J. Molemaker and J.C. McWilliams, "Submesoscale dynamics of a Gulf Stream frontal eddy in the South Atlantic Bight," *Journal of Physical Oceanography*, **46** (2016), 305-325.

[20] A. Hadjighasem, M. Farazmand, D. Blazevski, G. Froyland and G. Haller, "A critical comparison of Lagrangian methods for coherent structure detection," *Chaos: An Interdisciplinary Journal of Nonlinear Science*, **27(5)** (2017)

[21] A. Hadjighasem, D. Karrasch, H. Teramoto and G. Haller, "Spectral-clustering approach to Lagrangian vortex detection," *Physical Review E*, **93** (2016)

[22] G. Haller, Lagrangian coherent structures. *Ann. Rev. Fluid Mech.* **47** (2015) 137-162.

[23] G. Haller, "Dynamically consistent rotation and stretch tensors from a dynamic polar decomposition," *J. Mechanics and Physics of Solids*, **80** (2016) 70-93.

[24] G. Haller, A. Hadjighasem, M. Farazmand and F. Huhn, "Defining coherent vortices objectively from the vorticity." *J. Fluid Mech.* **795** (2016) 136-173.

[25] G. Haller, N.O. Aksamit, and A. P. Encinas-Bartos, "Quasi-objective coherent structure diagnostics from single trajectories," *Chaos: An Interdisciplinary Journal of Nonlinear Science* **31** (2021).

[26] G. Haller, N. O. Aksamit and A.P. Encinas-Bartos, "Erratum: Quasi-objective coherent structure diagnostics from single trajectories," *https://arxiv.org/pdf/2101.05903.pdf* (in press (2022))

[27] D. Kang and E.N. Curchitser, "Gulf Stream eddy characteristics in a high-resolution ocean model," *Journal of Geophysical Research: Oceans*, **118** (2013), 4474–4487.

[28] M. Lévy, P.J. Franks and K.S. Smith, "The role of submesoscale currents in structuring marine ecosystems," *Nature communications*, **9** (2018), 1–16.

[29] J.M.Lilly and S.C. Olhede, "Bivariate instantaneous frequency and bandwidth," *IEEE Transactions on Signal Processing*, **58** (2009), 591–603.

[30] J.M.Lilly and S.C. Olhede, "On the analytic wavelet transform," *IEEE transactions on information theory*, **56(8)**, 4135-4156.

[31] J. M.Lilly and P. Pérez-Brunius, "Extracting statistically significant eddy signals from large Lagrangian datasets using wavelet ridge analysis, with application to the Gulf of Mexico," *Nonlinear Processes in Geophysics*, **28** (2021), 181–212.

[32] R. Lumpkin, A. M. Treguier and K. Speer, "Lagrangian eddy scales in the northern Atlantic Ocean," *Journal of physical oceanography*, **32(9)** (2002), 2425-2440.

[33] R. Lumpkin and M. Pazos, "Measuring surface currents with Surface Velocity Program drifters: the instrument, its data, and some recent results," *Lagrangian analysis and prediction of coastal and ocean dynamics*, **39** (2007), 67.

[34] R. Lumpkin and G. C. Johnson, "Global ocean surface velocities from drifters: Mean, variance, El Niño-Southern Oscillation response, and seasonal cycle," *Journal of Geophysical Research: Oceans*, **118(6)** (2013), 2992-3006.

[35] R. Lumpkin, "Global characteristics of coherent vortices from surface drifter trajectories," *Journal of Geophysical Research: Oceans*, **121** (2016), 1306–1321.

[36] J. Martínez-Moreno A. M. Hogg, A. E. Kiss, N. C. Constantinou and A. K. Morrison, "Kinetic Energy of Eddy-Like Features From Sea Surface Altimetry," *Journal of Advances in Modeling Earth Systems*, **11(10)**, 3090-3105.

[37] A.M. Mancho, S. Wiggins, J. Curbelo and C. Mendoza, "Lagrangian descriptors: A method for revealing phase space structures of general time dependent dynamical systems," *Communications in Nonlinear Science and Numerical Simulation*, **18** (2013), 3530–3557.

[38] C. Mendoza, A.M. Mancho, and S. Wiggins, "Lagrangian descriptors and the assessment of the predictive capacity of oceanic data sets", *Nonlinear Processes in Geophysics*, **21(3)** (2014), 677-689.

[39] C. Mendoza and A.M. Mancho, "Hidden geometry of ocean flows," *Physical review letters*, **105(3)** (2010), 038501.

[40] A.J. Mariano, E.H. Ryan, H.S. Huntley, L.C Laurindo, E. Coelho, A. Griffa, ... and M. Wei, "Statistical properties of the surface velocity field in the northern Gulf of Mexico sampled by GLAD drifters," *Journal of Geophysical Research: Oceans*, **121** (2016), 5193–5216.

[41] McWilliams, J. C, "Submesoscale currents in the ocean," *Proceedings of the Royal Society A: Mathematical, Physical and Engineering Sciences*, **472** (2016), 20160117.

[42] P. Miron, M.J. Olascoaga, F.J. Beron-Vera, N.F. Putman, J. Triñanes, R. Lumpkin and G.J. Goni, "Clustering of Marine Debris and Sargassum Like Drifters Explained by Inertial Particle Dynamics," *Geophysical Research Letters*, **47** (2020).

[43] S. Mowlavi, M. Serra, E. Maiorino and L. Mahadevan, "Detecting Lagrangian coherent structures from sparse and noisy trajectory data," arXiv preprint (2021).

[44] R. Mundel, E. Fredj, H. Gildor and V. Rom-Kedar, "New Lagrangian diagnostics for characterizing fluid flow mixing", *Phys. Fluids* **26**, 126602 (2014)

[45] G. Novelli, C.M. Guigand, C. Cousin, E.H. Ryan, N.J. Laxague, H. Dai, B.K. Haus and T.M. Özgökmen, "A biodegradable surface drifter for ocean sampling on a massive scale," *Journal of Atmospheric and Oceanic Technology*, **34(11)** (2017), 2509–2532.

[46] M.J. Olascoaga., F.J. Beron-Vera, G. Haller, J. Triñanes, M. Iskandarani, E. F. Coelho, B.K. Haus, H.S. Huntley, G. Jacobs, A.D. Kirwan and B.L. Lipphardt, "Drifter motion in the Gulf of Mexico constrained by altimetric Lagrangian coherent structures," *Geophysical Research Letters* **40** (2013): 6171–6175.

[47] M.J. Olascoaga and G. Haller, "Forecasting sudden changes in environmental pollution patterns," *Proceedings of the National Academy of Sciences*, **109** (2012), pp.4738-4743.

[48] A. C. Poje, T.M. Özgökmen, B.L. Lipphardt, B.K. Haus, E.H. Ryan, A.C. Haza, ... and A. J. Mariano, "Submesoscale dispersion in the vicinity of the Deepwater Horizon spill," *Proceedings of the National Academy of Sciences*, **111(35)** (2014) , 12693-12698.

[49] A. Provenzale, "Transport by coherent barotropic vortices," *Annual review of fluid mechanics*, **31**, pp.55–93.

[50] P.L. Richardson, A.E. Strong and J.A. Knauss, "Gulf Stream eddies: Recent observations in the western Sargasso Sea. *Journal of Physical Oceanography*," **3** (1973), 297–301.

[51] P.L. Richardson, "Eddy kinetic energy in the North Atlantic from surface drifters," *Journal of Geophysical Research: Oceans*, **88(C7)** (1983), 4355-4367.

[52] P.L. Richardson, "A census of eddies observed in North Atlantic SOFAR float data," *Progress in Oceanography*, **31(1)** (1993), 1-50.

[53] T. Rossby, M. Omand, J. Palter and D. Hebert, "On rates of isopycnal dispersion at the submesoscale," *Geophysical Research Letters*, **48** (2021).

[54] A. Ruiz-Herrera, "Some examples related to the method of Lagrangian descriptors," *Chaos: An Interdisciplinary Journal of Nonlinear Science*, **25(6)** (2015), 063112.

[55] A. Ruiz-Herrera, "Performance of Lagrangian descriptors and their variants in incompressible flows," *Chaos: An Interdisciplinary Journal of Nonlinear Science* **26(10)** (2016): 103116.

[56] I.I. Rypina, S.E. Scott, L.J. Pratt and M.G. Brown, "Investigating the connection between complexity of isolated trajectories and Lagrangian coherent structures," *Nonlin. Proc. Geophys.* **18** (2011) 977–987.

[57] B.L. Sawford, "Rotation of trajectories in Lagrangian stochastic models of turbulent dispersion," *Boundary-layer meteorology*, **93** (1999), pp.411–424.

[58] K. L. Schlueter-Kuck and J.O. Dabiri, "Coherent structure colouring: identification of coherent structures from sparse data using graph theory," *Journal of Fluid Mechanics*, **811** (2017), 468-486.

[59] T.G. Shepherd, J.N. Koshyk and K. Ngan, "On the nature of large-scale mixing in the stratosphere and mesosphere," *Journal of Geophysical Research: Atmospheres* **105(D10)** (2000): 12433-12446.

[60] O.R. Southwick, E.R. Johnson and N.R. McDonald, "A simple model for sheddies: Ocean eddies formed from shed vorticity," *Journal of Physical Oceanography*, **46** (2016), pp.2961–2979.

[61] O. R. Southwick, E.R. Johnson and N.R. McDonald, "Potential vorticity dynamics of coastal outflows," *Journal of Physical Oceanography*, **47** (2017), 1021–1041.

[62] N. Tarshish, R. Abernathey, C. Zhang, C.O. Dufour, I. Frenger and S.M. Griffies, "Identifying Lagrangian coherent vortices in a mesoscale ocean model," *Ocean Modelling*, **130** (2018), pp.15–28.

[63] E. van Sebille, M.H. England and G. Froyland, "Origin, dynamics and evolution of ocean garbage patches from observed surface drifters," *Environmental Research Letters*, **7** (2012).

[64] M. Veneziani, A. Griffa, A.M. Reynolds and A.J. Mariano, "Oceanic turbulence and stochastic models from subsurface Lagrangian data for the Northwest Atlantic Ocean," *Journal of physical oceanography*, **34(8)** (2004), 1884-1906.

[65] M. O. Williams, I.I. Rypina and C.W. Rowley, "Identifying finite-time coherent sets from limited quantities of Lagrangian data," *Chaos: An Interdisciplinary Journal of Nonlinear Science*, **25** (2015), 087408.